12th International Workshop on Wave Hindcasting and Forecasting, Kohala Coast, Hawai'i, HI, 2011.

A Thirty Year Wave Hindcast Using The Latest NCEP Climate Forecast System Reanalysis Winds[1]

Arun Chawla[2,*], Deanna Spindler[†], Hendrik L. Tolman[*]
[*]NOAA/NCEP Environmental Modeling Center, Camp Springs MD
[†]IMSG at NOAA/NCEP

1 INTRODUCTION

A long-term global wave database is very useful to build wave climatologies, do scenario studies as well as undertake model validation analysis across multiple time scales. The wave modeling group at the National Center for Environmental Prediction (NCEP) maintains a wave hindcast database that extends from 1999 to the present. This database uses the archived analysis winds from the GFS atmospheric model (Moorthi et al., 2001) to drive the waves. However, this database is inconsistent because all the numerical and physical upgrades to the models (both wave and atmosphere) are tied in with the variability of the underlying physics. This can be countered by doing a reanalysis so that the same model can be used to build a consistent multi-decadal database.

There is not enough available data to develop a traditional re-analysis of the wave environment. Furthermore, wave dynamics are different from atmospheric dynamics in the sense that they are more of a boundary value problem than an initial value problem, with the wind forcing being the most dominant process driving wave dynamics. Thus, it is more useful to do a hindcast re-run using a reanalysis wind field. However, till now the reanalysis winds developed at NCEP were on too coarse a grid to allow for the development of a meaningful wave hindcast database.

A new NCEP Climate Forecast System Reanalysis Reforecast (CFSRR) system has been recently developed and entails a coupled reanalysis of the atmospheric, oceanic, sea-ice and land data from 1979 through 2010, and a reforecast run with this reanalysis (Saha et al., 2010). This reanalysis has much higher horizontal and vertical resolution of the atmosphere than the Global and the North American Reanalysis, and can thus be used to develop a long-term hindcast wave database.

The wave model used at NCEP is a third generation wind wave model WAVEWATCH III® (Tolman, 2009). In 2007, the model was expanded to run as a mosaic of two–way nested grids (Tolman, 2008). The nested grid driver is described in Tolman (2007a,b), and the grid generation tools used to develop these grids are described in Chawla and Tolman (2007, 2008). To drive the waves the wave model requires two input fields: ice and winds (including the air-sea temperature difference). The high resolution winds used here are 10m above sea level on an hourly temporal and 1/2° spatial resolution which cover the globe from 90°S–90°N. The reanalysis daily ice concentration fields are 1/2° spatial resolution, and are derived from passive microwave from the SMMR and SSMI using the NASA Team algorithm.

This hindcast database is foreseen to be developed in three stages. In the first stage, the wave model shall be run (for the 30 year hindcast period from 1979 to 2009) using the same physics packages that are currently used in NCEP operations (with minor exceptions these are also the default settings described in Tolman (2009)). This will set the baseline for the wave model. The database will be regenerated in stage 2 and 3 with newer physics packages as they become available, courtesy of a concurrent NOPP initiative to improve physics in operational wind wave models. However, the model setup and products will remain unchanged at the different

[1]MMAB Contribution No. 296
[2]arun.chawla@noaa.gov
[3]This may change depending on developments in model capability and/or database generation

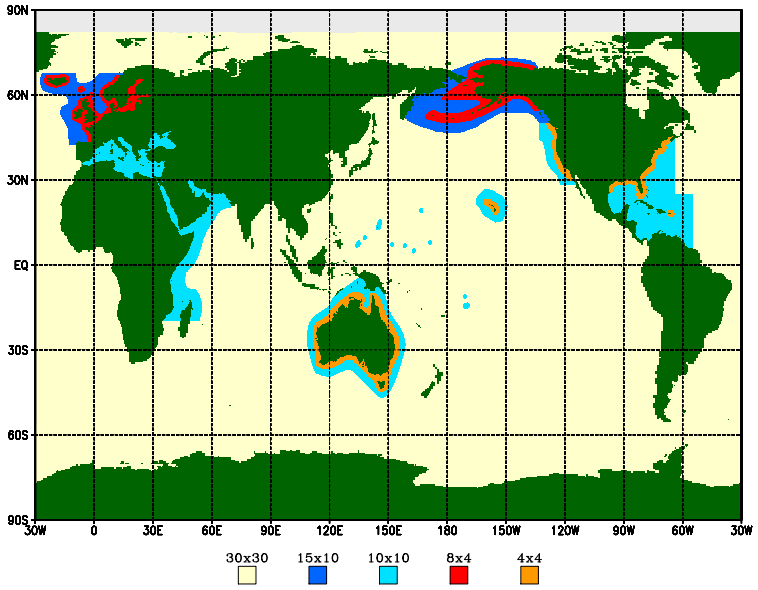

Fig. 1 : Global domain. Grid resolution given in arc-minutes.

stages[3].

The first stage of this hindcast database has just been completed and the purpose of this paper is to provide a detailed report on the model setup and products as well as some validation of the wind and wave records. The second stage of the database is scheduled to begin later this year and will include the physics package of Ardhuin et al. (2010). It will cover the same time period as the first stage (1979–2009). A separate paper in this conference (Ardhuin et al., 2011a) also addresses hindcasts using CFSRR winds and Ardhuin et al. (2010) physics.

2 MODEL SETUP

2.a Grids

The WAVEWATCH III model can be run as a mosaic of grids with two–way interaction between the higher and lower resolution grids. This facilitates increased computational efficiencies by restricting the higher resolution grids only in the necessary areas.

Keeping in mind the requirements of our collaborative partners, a set of nested grids was produced for the global domain. In all the grids, the full resolution ETOPO1 bathymetry (Amante and Eakins, 2009) was used as the reference grid. See Chawla and Tolman (2007, 2008) for details on the software used for developing these grids.

Overall, the global domain was separated into sixteen computational grids (Fig. 1). Individual grid details are provided in Table 1. Grids of three different resolutions were generated: low resolution (1/2 ° or 30 arc-minutes), mid resolution (1/6° or 10 arc-minutes), and high resolution (1/15° or 4 arc-minutes). The 30 arc-minute grids cover the entire globe (in longitude) and are referred to as global grids. In this current implementation, we are using regular spherical grids[4] and as a result, model time steps are limited by the CFL limit near the poles. For increased efficiency, the global domain was divided into three "bands" . These three grids are primarily used for computation purposes, and the output from these grids is stored in a single global grid referred to as **glo_30m** (this grid is only used for merging output from the global grids **ao_30m**, **mid_30m**, **ac_30m** and not for computations).

To avoid the singularity at the poles, all grid points beyond 82° N in the Arctic grid (**ao_30m**) are marked as inactive. This is not an issue in the Antarctic grid (**ac_30m**) because of land cover at the South Pole.

Nested inside the low resolution grids are the intermediate grids, which have been masked so that the

[4]both an unstructured and a curvilinear grid version of the model is currently under development and depending upon progress may be involved in the later stages of the database development

Table 1: WAVEWATCH III grid particulars. All output data associated with a particular grid are identified by their grid labels.

Name	Grid label	Latitude	Longitude	Resolution (lat x lon)
Global	glo_30m	$90°S : 90°N$	$180°E : 180°W$	1/2° x 1/2°
Arctic	ao_30m	$55°N : 90°N$	$180°E : 180°W$	1/2° x 1/2°
Mid-Globe	mid_30m	$65°S : 65°N$	$180°E : 180°W$	1/2° x 1/2°
Antarctic	ac_30m	$90°S : 55°S$	$180°E : 180°W$	1/2° x 1/2°
East Coast US	ecg_10m	$0°N : 55°N$	$100°W : 50°W$	1/6° x 1/6°
West Coast US	wc_10m	$25°N : 50°N$	$150°W : 110°W$	1/6° x 1/6°
Alaska	ak_10m	$44°N : 75°N$	$140°E : 120°W$	1/6° x 1/4°
Pacific Isl.	pi_10m	$20°S : 30°N$	$130°E : 145°W$	1/6° x 1/6°
Australia	oz_10m	$50°S : 0°N$	$105°E : 165°E$	1/6° x 1/6°
North Sea	nsb_10m	$42°N : 75°N$	$28°W : 31°E$	1/6° x 1/4°
Mediterranean	med_10m	$30°S : 48°N$	$7°W : 43°E$	1/6° x 1/6°
NW Indian O.	nwio_10m	$20°S : 31°N$	$30°E : 70°E$	1/6° x 1/6°
East Coast US	ecg_4m	$15°N : 47°N$	$101°W : 60°W$	1/15° x 1/15°
West Coast US	wc_4m	$15°N : 50°N$	$165°W : 116°W$	1/15° x 1/15°
Alaska	ak_4m	$48°N : 74°N$	$165°E : 122°W$	1/15° x 2/15°
Australia	oz_4m	$50°S : 0°N$	$105°E : 165°E$	1/15° x 1/15°
North Sea	nsb_4m	$42°N : 68°N$	$28°W : 31°E$	1/15° x 2/15°

only active points are those within approximately 250 NM from shore. In this resolution, Hawaii is part of the Pacific Islands grids.

The highest resolution grids are the 4 arc-minute coastal grids, masked so that the only active points are those within approximately 100 km of shore. In this resolution, Hawaii is part of the West Coast US grid. Since these grids can be computationally very expensive, they have been limited to regions of highest priority.

The spectral domain has been divided into 50 frequency and 36 directional bins (directional resolution of 10°). The minimum frequency has been set at 0.035 Hz and the frequency increment factor has been set at 1.07, providing a frequency range of 0.035–0.963. A parametric tail is fitted beyond the highest computed frequency.

2.b Physics Packages

At the first stage of the database development, the standard physics packages that are currently in operations at NCEP are used [5]. The physics package used are as follows

- The Tolman - Chalikov source term package (Tolman and Chalikov, 1996) with stability correction and a cap for maximum drag.
- DIA approximation for non-linear interactions.
- Battjes-Janssen shallow water depth breaking with a Miche-style shallow water limiter for maximum energy.
- ULTIMATE QUICKEST propagation scheme with averaging technique for Garden Sprinkler alleviation.
- JONSWAP bottom friction formulation with no bottom scattering

2.c Products

Two types of output products are generated by the wave model—field output that is produced on the model grid layout and point output that is produced at select locations. The aim of this database is to not only produce a long term data set for validation purposes, but also provide detailed spectral information at select locations to build climatologies and serve as boundary conditions for other modeling efforts. As a result, point output locations have been selected that correspond to known buoy locations as well as additional locations that were specifically requested

[5]Operational wave model at NCEP is being upgraded to use the new physics packages outlined in Ardhuin et al. (2010)

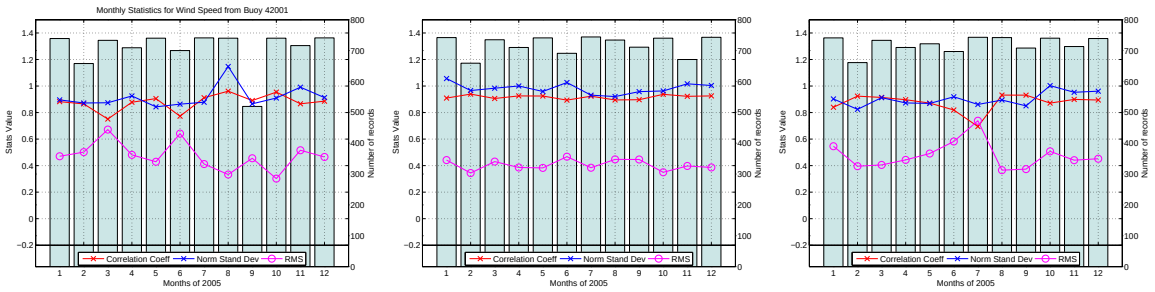

(a) Buoy 42001 (b) Buoy 46002 (c) Buoy 51001

Fig. 2: CFSRR wind statistics for the months of 2005. Error statistics are computed on a month by month basis and the vertical bars indicate the number of samples in any given month. Here the normalized standard deviation refers to the standard deviation in model winds normalized by the standard deviation in data.

by our collaborators. In all over two thousand output points have been selected. The output products generated on the grids are:

- Wind speed and direction as well as bulk spectral parameters—Significant wave height (Hs), Peak period (Tp) and Mean Direction at the peak period (Dp). These are stored in GRIB2 format with separate files for each parameter. Temporal resolution for the GRIB2 data is every 3 hours.
- Spectral partition data at all the grid output points. (Exception being the 30 arc-minute global grids where the output is stored at every other point). Temporal resolution for the partition data is every hour.

The temporal resolution of all products generated at the output points is hourly and the list of products are:

- The complete 2D spectra at each output point.
- Bulk spectral parameters using the WMO format at each output point. This includes the wind speed and direction, significant wave height and peak period.
- Partitioned wave data at the output points.

In the event that the output point is located in more than one grid, the energy spectrum is extracted from the finest grid that the point resides in. Linear interpolation is used to generate the spectrum at the output point from the neighboring grid points in the case that the output location does not correspond to a computational point.

Apart from these two types of products wave output is also generated along the altimeter tracks for later validation. This is done by interpolating in time and space wave parameters (significant wave height and wind speed) from the hourly field output files on to the altimeter tracks The altimeter tracks are obtained from the quality controlled global altimeter data set that is maintained at the French Research Institute for the Exploration of the Sea – IFREMER (Queffeulou, 2004).

3 CFSRR WINDS

The new NCEP Climate Forecast System Reanalysis Reforecast (CFSRR) entails a coupled reanalysis of the atmospheric, oceanic, sea-ice and land data from 1979 through 2010, and a reforecast run with this reanalysis (Saha et al., 2010). Here, only the reanalysis results will be used. The CFSRR has a much higher horizontal and vertical resolution of the atmosphere than the Global and the North American Reanalyses. The high resolution winds used here are 10m hourly with 1/2° spatial resolution, and cover the globe from 90°S–90°N.

The wind statistics for select buoys during 2005 are shown in Fig. 2. The correlation coefficient and the normalized standard deviation provide an estimate on how well the wind data are represented by the CFSRR database. Taylor diagrams are a convenient tool to plot normalized standard deviation, correlation coefficients and RMS errors on a single plot. Fig. 3 shows the Taylor diagrams for the different buoys at three different months in 2005. In this figure, the solid black contours represent the normal-

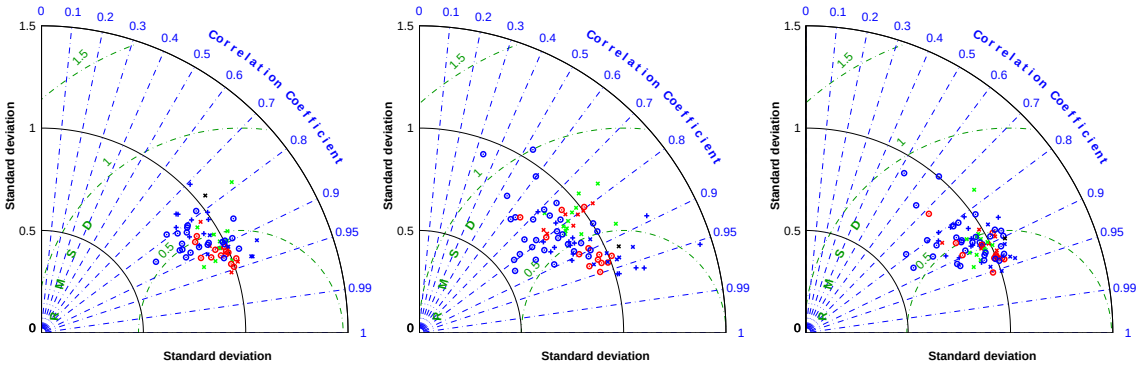

(a) March, 2005 (b) August, 2005 (c) December, 2005

Fig. 3: Taylor diagrams for the different ocean buoys. Buoys are color coded according to the basin they lie in. 'Red x' North Atlantic ; 'Blue x' North East Atlantic ; 'Green x' North west Atlantic ; 'Black x' South Atlantic ; 'Red o' North Pacific ; 'Blue o' North East Pacific ; 'Green o' North West Pacific ; 'Black o' South Pacific ; 'Blue +' Gulf of Mexico and Caribbean

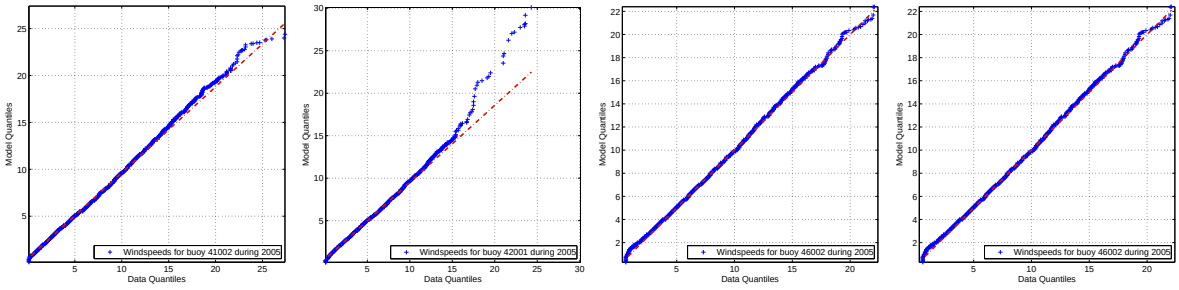

(a) Buoy 41002 (b) Buoy 42001 (c) Buoy 46002 (d) Buoy 51001

Fig. 4: Q–Q plot of wind speeds at select buoys for 2005 at four select buoys. Buoy 41002 is off the US East Coast approx 250 NM east of Charleston, SC. Buoy 42001 is in the deep waters of the Gulf of Mexico. Buoy 46002 is off of the US West Coast approximately 275 NM west of Coos Bay, OR. Buoy 51001 is near Hawaii approximately 170 NM West Northwest of Kauai island.

ized standard deviation, the dash dot blue lines represent the correlation coefficient and the dash dot green lines represent the RMS error. A perfect rendition of the data would yield a correlation coefficient and normalized standard deviation of 1 and an RMS error of 0. The data would then reside along the x-axis on the solid circle contour corresponding to a normalized standard deviation of 1. The closer all the data is to this point the better is the representation of the model. The figure shows that for most of the buoys the correlation is between 0.8 and 0.9 with the RMS error being around 0.5 m/s. A quantile - quantile (or Q–Q) plot can provide a very good comparison of the probability distribution of wind speeds between model and data. Fig. 4 shows the Q–Q plots for 2005 for four different buoys. All the buoys indicate that the wind speed magnitudes are well represented in CFSRR. The only exception is buoy 42001 where the CFSRR seems to be over predicting the higher wind speeds. This is reflected in the higher standard deviation values for the Gulf buoys during August 2005 in Fig. 3, and is probably an over representation of the winds during hurricane season. But by and large the winds are well represented by the CFSRR.

An additional quick test on the homogeneity of the wind fields for the entire 30 year period was performed by computing various monthly percentile wind speeds for the Northern and Southern Hemisphere mid latitude. Such an analysis has previously linked changes in model biases in the Southern Hemisphere to changes in the higher wind speeds (Chawla et al, poster presentation, 2010 WISE meeting, Brest, France). Results are presented in Fig. 5. For the Northern Hemisphere consistent behavior is observed for the entire 30 year period. Some variability is found in the highest percentile winds, but this variability appears to have a random nature as would be expected. For the Southern Hemisphere however, three distinct periods can be identified with discontinuously changing behavior of the higher percentile winds. The separations between periods occur around 1995 and 2007. Because the underlying models and analysis systems are kept constant throughout the entire reanalysis, the discontinuities are most likely due to the availability of individual data sources. This behavior will be investigated in more detail at NCEP.

4 VALIDATION

Validation has been done using the quality controlled altimeter data archive maintained at IFREMER (Queffeulou, 2004) as well as the NDBC archive. Some initial results are shown below.

One of the products generated by the monthly hindcast runs are model results collocated along the altimeter tracks. For each of the sixteen computational grids, hourly gridded model results are interpolated on to altimeter tracks that cross through the gridded domain. For the analysis, collocated data from all the different grids is used with the highest resolution data being used in areas of overlapping grids. This was used to build error maps such as the one shown in Fig. 6. Before computing the errors the altimeter data set was smoothed using a 15 point running average along the tracks.

Error statistics were computed for the collocated data sets in three month segments to get a sense of the seasonal and inter annual variabilities in model performance over the database. Fig. 7 shows the error statistics from all the different altimeters over the global domain. The errors show some interesting patterns. The Scatter Indices are generally lower after 2000, indicating a reduction in the random error in the models. This is probably related to a better representation of the wind due to additional sources of data for assimilation. The reduction in Scatter Indices are accompanied by a corresponding increase in the goodness of fit parameter (R^2). Biases on the other hand show some interesting patterns. Apart from the seasonal patterns (highs during the winter months in the Northern and Southern Hemispheres) there are some significant inter annual variabilities. Since these variabilities are seen across the different instruments (with some small differences) it is not a problem with the data but a pattern in the wave model. The overall RMS Error shows similar inter annual features, indicating that the biases make up a significant portion of the overall error.

Statistics from collocated tracks were also computed on a region by region basis to get an idea of where the errors were most prominent. Fig. 8 shows the bias patterns in the Northern and Southern Hemispheres. The seasonal bias patterns are visible in the Northern Hemisphere with the biggest biases occurring during the winter months. These are caused primarily by inadequate swell dissipation in the current formulation of WAVEWATCH III (Ardhuin et al., 2010; Chawla et al., 2009) and are most prominent in the Pacific Ocean (where the biggest swells are observed). The Southern Hemisphere shows a similar seasonal variability during the winter months. The inter annual variability that was observed in

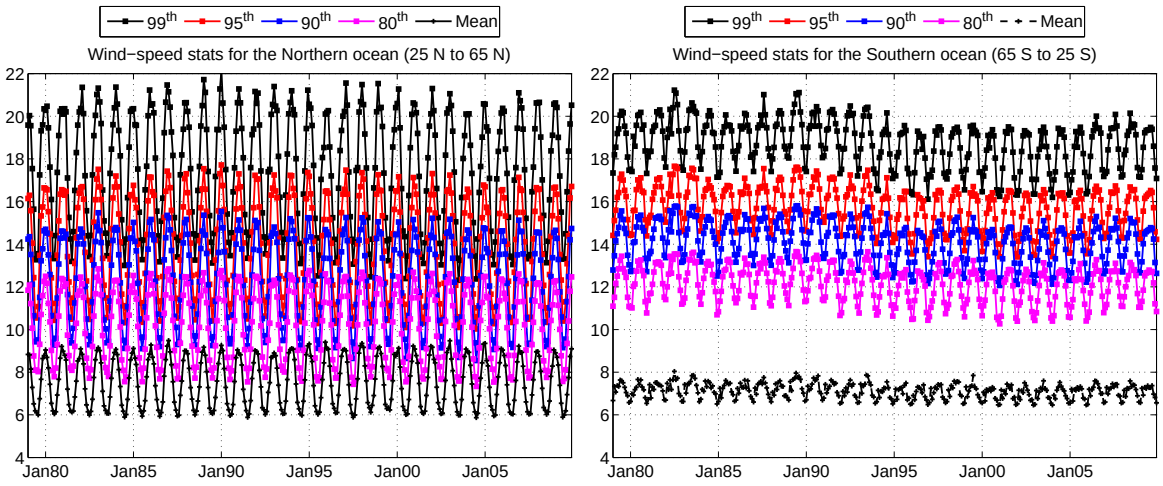

Fig. 5 : Monthly wind speed percentiles from the CFSRR database

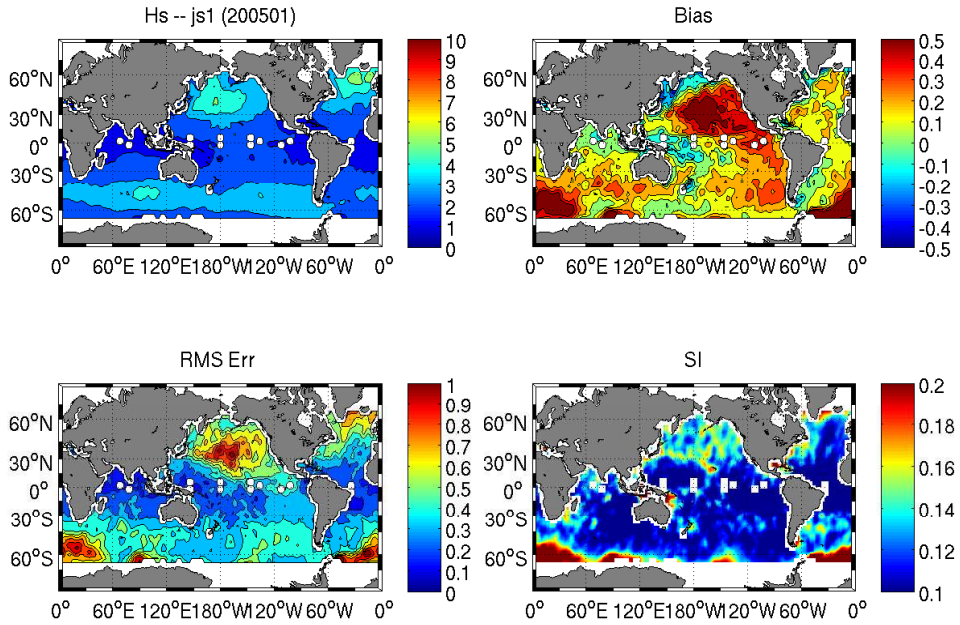

Fig. 6: Error map of Hs using the Jason-1 satellite data. Error maps are generated by binning the collocated data into 2° × 2° bins. For this map data from a three month period (Dec, 2004 through Feb, 2005) is used to provide enough points per bin for statistical analysis.

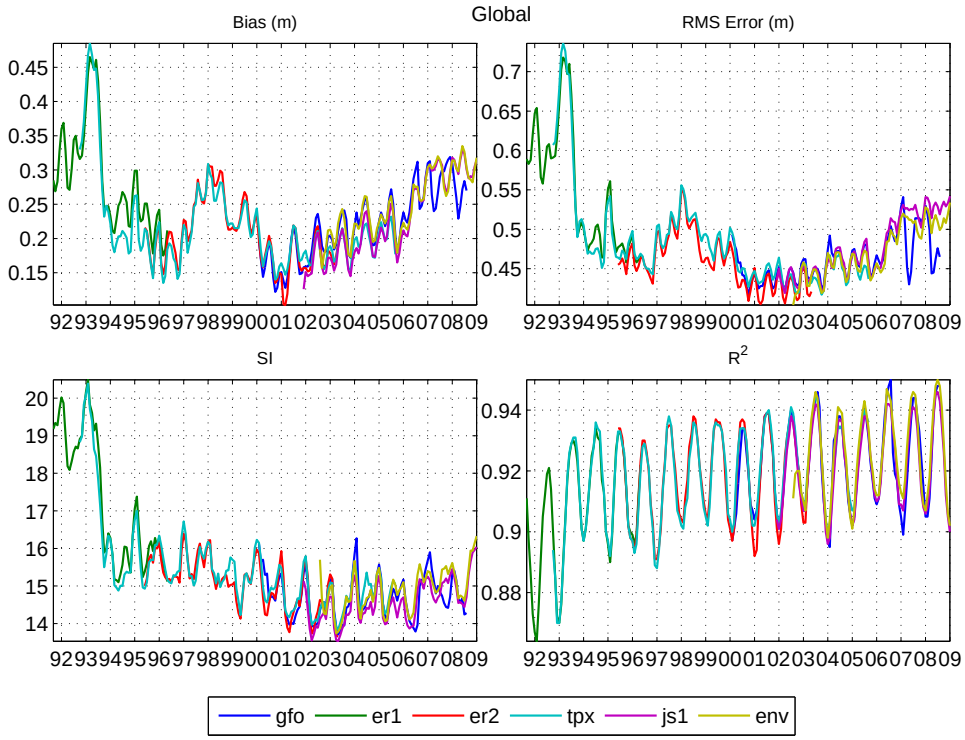

Fig. 7: Error Statistics from the different altimeters as a function of time from 1993 to 2009. Error statistics are computed over a sliding three month period for the global domain.

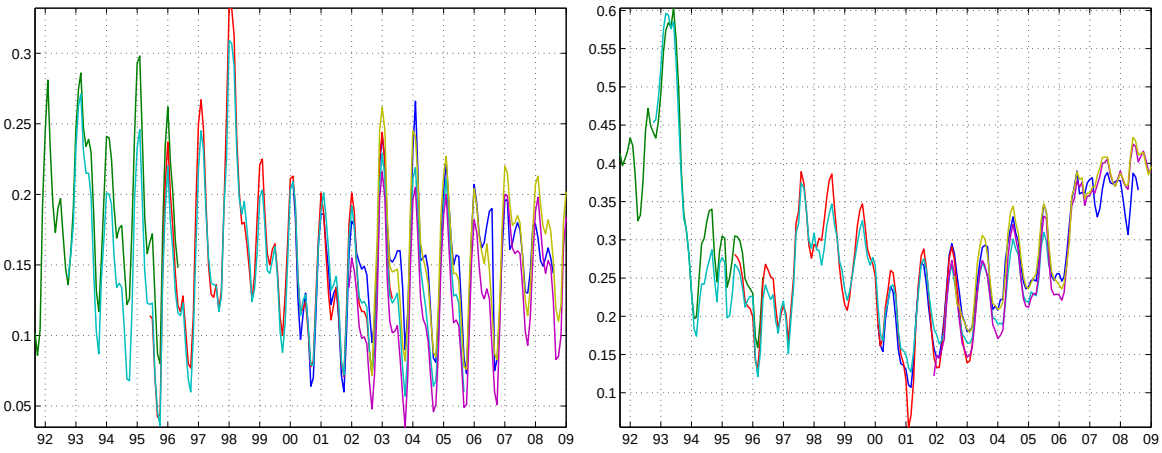

(a) N Hemisphere

(b) S Hemisphere

Fig. 8: Hs biases from the different altimeters for the Northern and Southern Hemispheres. Statistics are computed the same way as in Fig 7.

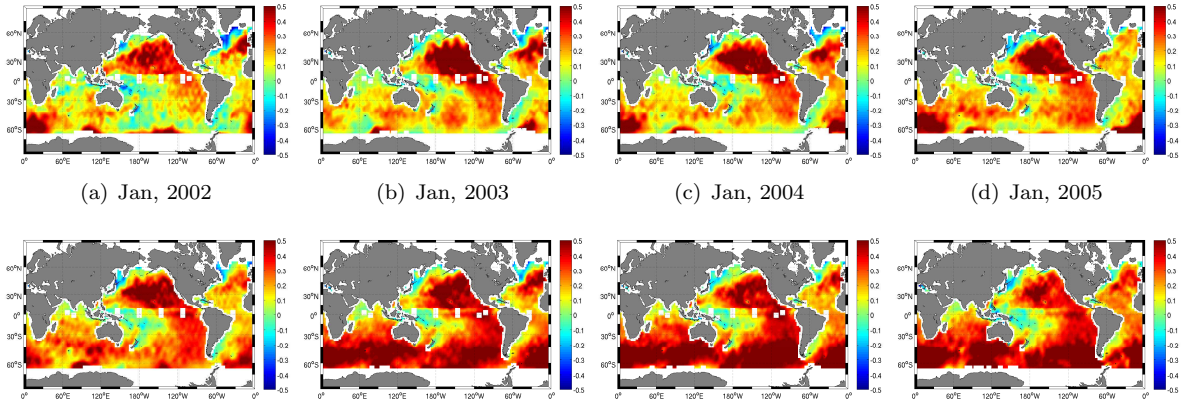

(a) Jan, 2002 (b) Jan, 2003 (c) Jan, 2004 (d) Jan, 2005

(e) Jan, 2006 (f) Jan, 2007 (g) Jan, 2008 (h) Jan, 2009

Fig. 9: Hs bias maps from the Jason 1 satellite tracks for the months of January (2002 – 2009). See Fig 6 for details on how the maps were generated

the global domain (Fig. 7), on the other hand, is only seen in the Southern Hemisphere. Fig 9 shows the impact of increasing bias in the Southern Hemisphere for the summer months of 2002 – 2009. The build up of biases occurs primarily along the western coast of South America and South of 45°S. The jump in biases in 2007 match the increase in Southern Hemisphere wind speeds (Fig. 5).

Buoy data analysis has only been done for a small subset of all the available buoy records. Figs 10 and 11 show the Taylor diagrams and Q–Q plots for select buoys in 2005. The correlation between model and data are excellent, with a correlation of 0.9 or higher for most times of the year. The highest waves, however, are under represented in the model.

5 CONCLUSIONS

A detailed thirty year database of wave hindcasts has been developed using the high resolution CFSRR winds from NCEP. The development of this database is part of a NOPP initiative to improve the representation of physical processes in operational third generation wind wave models. The database is envisioned to be completed in three stages, with each stage consisting of a complete thirty year hindcast. This paper reports the completion of the first stage of the database, built using the default physics package in WAVEWATCH-III. The next two stages are expected to be completed over the extent of the NOPP project.

The database has been constructed using sixteen two-way nested grids with resolution ranging from 1/2° to 1/15°. Products generated include bulk and partitioned spectral parameters over the domain of the grids as well as detailed spectral data at over 2000 output locations.

Validation studies show that the high temporal and spatial resolution CFSRR winds provide a very accurate estimate of the atmospheric conditions needed to build a climatological wave hindcast database. Winds in the Southern Hemisphere show some distinct variabilities over the thirty year period that are probably related to availability of data for assimilation in this region.

Initial comparison of buoy and altimeter data show that the waves are very well represented in the system. With the exception of 1993, and two other instances, the total RMS error in Hs is much less than 50 cm. The Northern Hemisphere shows seasonal bias patterns that are related to swell dissipation processes, but the Southern Hemisphere shows considerable inter annual variability. Some of the earlier bias seen in the altimeter comparisons are probably related to the availability of data for assimilation in this region. Ardhuin et al. (2011a) have reported unusually high bias for 1991 using CFSRR winds that are still unexplained. Some of the high biases that are seen for 1993 in this paper may be related to the same issue. Analysis with buoy data has been done only for a limited set but show a negative bias in the model for the higher waves. A similar result has also been found by Ardhuin et al. (2011a) using the altimeter data sets. Of particular interest are the inter annual variations in biases in the Southern Hemisphere. There are multiple possible reasons for this. First, reanalysis winds in the Southern Hemisphere have only a limited set of satellite data available

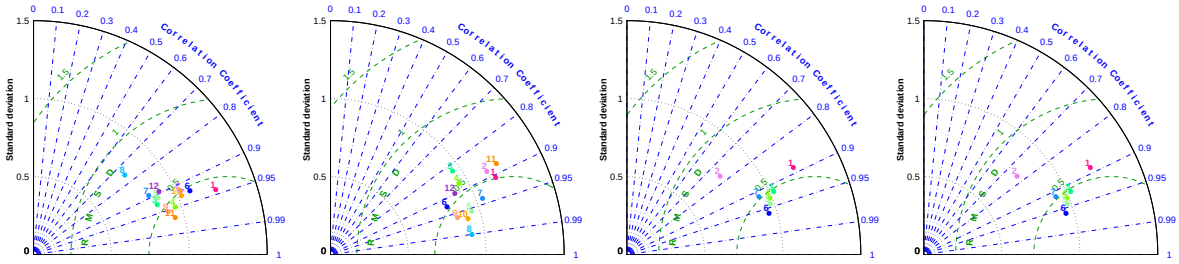

(a) Buoy 41002 (b) Buoy 42001 (c) Buoy 46002 (d) Buoy 51001

Fig. 10: Taylor diagrams of Hs at select buoys for 2005. The colored dots with numbers refer to the different months in the year

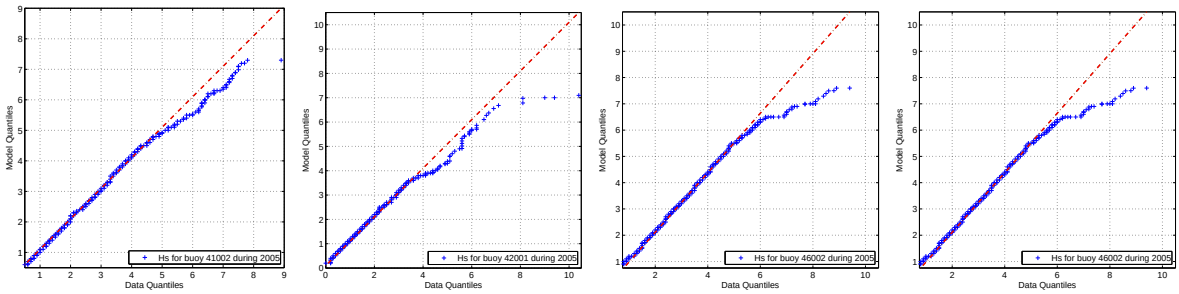

(a) Buoy 41002 (b) Buoy 42001 (c) Buoy 46002 (d) Buoy 51001

Fig. 11 : Q–Q plot of Hs at select buoys for 2005

for assimilation which make them particularly sensitive to changes in instruments and/or algorithms for retrievals. This can be seen in the variations of the highest percentile winds in the Southern Hemisphere. A second possible cause for inter annual variations in biases can be the treatment of icebergs in the model (Ardhuin et al., 2011b). These icebergs have considerable inter annual variability and can play an effective dampening role (Ardhuin et al., 2011b). The icebergs have not been accounted for at this stage of the hindcasts. Ardhuin et al. (2011a) have accounted for the icebergs for the period 2002–2009 in their hindcasts for which they report very little variability in the biases. This is different from the slow build up of biases observed here. The spatially intermittent nature of biases South of 45°S (Fig 9) provide further evidence that icebergs play an important role in determining bias patterns for the Southern Hemisphere. Thanks to the efforts of Fabrice Ardhuin and his team at IFREMER, the latest version of WAVEWATCH-III accounts for the effects of icebergs (Ardhuin et al., 2011b), and their impacts will be assessed in the second stage of the database development.

A more detailed analysis of this database will be carried out over the next few months, which will include further analysis on the nature of the winds, comparisons with buoy data, spectral comparisons using the IMEDS package (Devaliere and Hanson, 2009) as well as detailed studies of specific storms and hurricanes. The insight gained will be used to design the second stage of the database development which shall use the physics package of Ardhuin et al. (2010) and shall begin in early 2012.

References

Amante, C. and B. W. Eakins, 2009: Etopo1 1 Arc Minute Global Relief Model: Prodecures, Data Sources and Analysis. NOAA Technical Memorandum NGDC-24, NESDIS, 19 pp.

Ardhuin, F., J. Hanafin, Y. Quilfen, B. Chapron, P. Queffeulou, M. Obrebski, J. Sienkiewicz and D. Vande-

mark, 2011a: Calibration of the IOWAGA global wave hindcast (1991 - 2011) using ECMWF and CFSR winds. in *12th International Workshop on Wave Hindcasting and Forecasting, Kohala Coast, HI*, p. pp 11.

Ardhuin, F., E. Rogers, A. Babanin, J.-F. Filipot, R. Magne, A. Roland, A. V. Westhuysen, P. Queffeulou, J.-M. Lefevre, L. Aouf and F. Collard, 2010: Semi-empirical dissipation source functions for ocean waves: Part 1, definition, calibration and validation. *J. Phys. Oceanogr.*, **40**, 1917–1941.

Ardhuin, F., J. Tournadre, P. Queffeulou, F. Girard-Ardhuin and F. Collard, 2011b: Observation and parametrization of small icebergs: Drifting breakwaters in the southern ocean. *Ocean Modelling*, **39**, 405–410.

Chawla, A. and H. L. Tolman, 2007: Automated grid generation for WAVEWATCH III. Technical note 254, NCEP/NOAA/NWS, National Center for Environmental Prediction, Washington DC.

Chawla, A. and H. L. Tolman, 2008: Obstruction grids for spectral wave models. *Ocean Modeling*, In review.

Chawla, A., H. L. Tolman, J. L. Hanson, E.-M. Devaliere and V. M. Gerald, 2009: Validation of a multi-grid wavewatch iii modelling system. in *11th international workshop on wave hindcasting and forecasting & coastal hazards symposium, JCOMM Tech. Rep. 52, WMO/TD-No. 1533*.

Devaliere, E.-M. and J. Hanson, 2009: *IMEDS Interactive Model Evaluation and Diagnostics System V2.6 Users Guide*. US Army Corps of Engineers, Field Research Facility, Duck, NC.

Moorthi, S., H.-L. Pan and P. Caplan, 2001: Changes to the 2001 ncep Operational MRF/AVN Global Analysis/Forecast System. Technical Procedures Bulletin 484, NWS/NCEP.

Queffeulou, P., 2004: Long term validation of wave height measurement from altimeters. *Marine Geodesy*, **27**, 495–510.

Saha, S., S. Moorthi, H. Pan, X. Wu, J. Wang, S. Nadiga, P. Tripp, R. Kistler, J. Wollen, D. Behringer, H. Liu, D. Stokes, R. Grumbine, G. Gayno, J. Wang, Y. Hou, H. Chuang, H. Juang, J. Sela, M. Iredell, R. Treadon, D. Kleist, P. V. Delst, D. Keyser, J. Derber, M. Ek, J. Meng, H. Wei, R. Yang, S. Lord, H. van den Dool, A. Kumar, W. Wang, C. Long, M. Chelliah, Y. Xue, B. Huang, J. Schemm, W. Ebisuzaki, R. Lin, P. Xie, M. Chen, S. Zhou, W. Higgins, C. Zou, Q. Liu, Y. Chen, Y. Han, L. Cucurull, R. Reynolds, G. Rutledge and M. Goldberg, 2010: The NCEP climate forecast system reanalysis. *Bull. Am. Meteor. Soc.*, **91**, 1015–1057.

Tolman, H. L., 2007a: The 2007 release of WAVEWATCH III. in *10th international workshop on wave hindcasting and forecasting & coastal hazards symposium*. Paper Q4.

Tolman, H. L., 2007b: Development of a multi-grid version of WAVEWATCH III. Tech. Note 256, NOAA/NWS/NCEP/MMAB, 88 pp. + Appendices.

Tolman, H. L., 2008: A mosaic approach to wind wave modeling. *Ocean Modelling*, **25**, 35–47.

Tolman, H. L., 2009: User manual and system documentation of WAVEWATCH III version 3.14. Tech. Note 276, NOAA/NWS/NCEP/MMAB, 220 pp.

Tolman, H. L. and D. Chalikov, 1996: Source terms in a thrid generation wind wave model. *Journal of Physical Oceanography*, **26**, 2497–2518.